Cross-shell excitations near the "island of inversion": Structure of ^{30}Mg

A. N. Deacon,[1,*] J. F. Smith,[2] S. J. Freeman,[1] R. V. F. Janssens,[3] M. P. Carpenter,[3] B. Hadinia,[2] C. R. Hoffman,[4,†] B. P. Kay,[3] T. Lauritsen,[3] C. J. Lister,[3] D. O'Donnell,[2,‡] J. Ollier,[2,‡] T. Otsuka,[5,6] D. Seweryniak,[3] K.-M. Spohr,[2] D. Steppenbeck,[1,§] S. L. Tabor,[4] V. Tripathi,[4] Y. Utsuno,[7] P. T. Wady,[2] and S. Zhu[3]

[1]*Schuster Laboratory, University of Manchester, Manchester M13 9PL, United Kingdom*
[2]*University of the West of Scotland, High Street, Paisley PA1 2BE, United Kingdom*
[3]*Argonne National Laboratory, Argonne, Illinois 60439, USA*
[4]*Department of Physics, Florida State University, Tallahassee, Florida 32306, USA*
[5]*Department of Physics, University of Tokyo, Hongo, Bunkyo-ku, Tokyo 113-0033, Japan*
[6]*Center for Nuclear Study, University of Tokyo, Hongo, Bunkyo-ku, Tokyo 113-0033, Japan*
[7]*Japan Atomic Energy Agency, Tokai, Ibaraki 319-1195, Japan*

(Received 18 June 2010; published 7 September 2010)

Excited states in ^{30}Mg have been populated to $\sim 6\hbar$ and 5 MeV excitation energy with the ^{14}C(^{18}O,$2p$) reaction. Firm spin assignments for states with $J > 2\hbar$ have been made in this nucleus. The level scheme is compared to shell-model calculations using the Universal *sd* effective interaction and the Monte Carlo shell model method. Calculations employing a full *sd* model space fail to reproduce the observed levels. The results indicate that excitations across the $N = 20$ gap are required at relatively low excitation energy to achieve a description of the data. The incorporation of the $f_{7/2}$ and $p_{3/2}$ orbitals into the model space gives improved results but indicate the need for further refinement of the models to reproduce the observed spectra.

DOI: 10.1103/PhysRevC.82.034305 PACS number(s): 23.20.Lv, 23.20.En, 21.60.Cs, 25.70.Jj

I. INTRODUCTION

The "island of inversion" in the neutron-rich *sd* shell is a region of the nuclear chart where the effects of shell evolution in nuclei far from stability have been studied for over 30 years. Unexpectedly high binding energies, observed via mass measurements of ^{31,32}Na [1], were later reproduced in Hartree-Fock calculations when $\nu f_{7/2}$ intruder configurations were included [2]. The same effects were subsequently seen in $_{12}$Mg and $_{10}$Ne isotopes around $N = 20$ [3]. Systematic trends in $E(2_1^+)$ and $B(E2; 0^+_{\text{g.s.}} \rightarrow 2_1^+)$ values have added weight to the arguments for large deformation in the ground- and low-lying states of $N \sim 20$ isotones below $Z = 12$, while data for $_{14}$Si, $_{16}$S, $_{18}$Ar, and $_{20}$Ca nuclei are characteristic of a large $N = 20$ shell gap. Measured mean-square charge radii and magnetic moments for Na and Ne isotopes have confirmed the notion of a large deformation in these systems [4,5].

The large ground-state deformation of nuclei within the island of inversion is largely understood as resulting from deformed states of $f_{7/2}$ and $p_{3/2}$ spherical parentage falling below similar states arising from the $d_{3/2}$ orbital as the neutron number increases [6]. There may be several contributing factors causing such a significant drop in energy for the intruder state; recent theoretical efforts have focused on the monopole component of the nucleon-nucleon interaction [7,8], revealing that both the central and the tensor forces dominate shell evolution. The central force is always attractive, with similar strength between two d orbitals as for a d-and-f pair of states. The additional effect of the tensor force between protons and neutrons, however, is attractive between the $d_{5/2}$ ($j_>$) and the $d_{3/2}$ ($j_<$) orbitals and repulsive between the $d_{5/2}$ ($j_>$) and $f_{7/2}$ ($j_>$) states. As the central force is stronger than the tensor force, the net effect is that of an attraction between both the $\pi d_{5/2}$ and $\nu d_{3/2}$ and the $\pi d_{5/2}$ and $\nu f_{7/2}$ orbitals, but less so in the latter case. For neutron-rich Ne, Na, and Mg isotopes, these effects conspire to reduce the size of the $N = 20$ gap, resulting in collectivity at low excitation energy, or even in the ground states, as highlighted earlier.

The current work focuses on ^{30}Mg, an isotope lying at the boundary of the island of inversion. Recent neutron-knockout experiments have confirmed this by contrasting the spectroscopic strength associated with the negative-parity orbitals in the ground states of ^{30}Mg and ^{32}Mg [9]. The strength in ^{30}Mg is a third of that found in ^{32}Mg, highlighting a dramatic change when entering the region of inversion. ^{30}Mg is, therefore, not expected to have significant ground-state deformation. However, the $N = 20$ gap should be smaller than for stable nuclides and, as such, configurations involving the $\nu f_{7/2}$ and $\nu p_{3/2}$ orbitals should be observed at relatively low excitation energy. If intruder configurations involve $\nu f^2_{7/2}$ excitations, enhanced proton-neutron interactions may lead to collectivity in these excited states.

This article presents a study of ^{30}Mg by a fusion-evaporation reaction. The statistics collected in recoil-gated γ-ray spectra, and the quality of the information on the states in the resulting level scheme, are in line with those determined for previous $2p$ channels, ^{59,60}Cr [10,11], obtained with this

*alick.deacon@manchester.ac.uk
†Current address: Argonne National Laboratory, Argonne, IL 60439, USA.
‡Current address: STFC Daresbury Laboratory, Warrington, WA4 4AD, UK.
§Current address: RIKEN Nishina Center, 2-1 Hirosawa, Wako-shi, Saitama 351-0198, Japan.

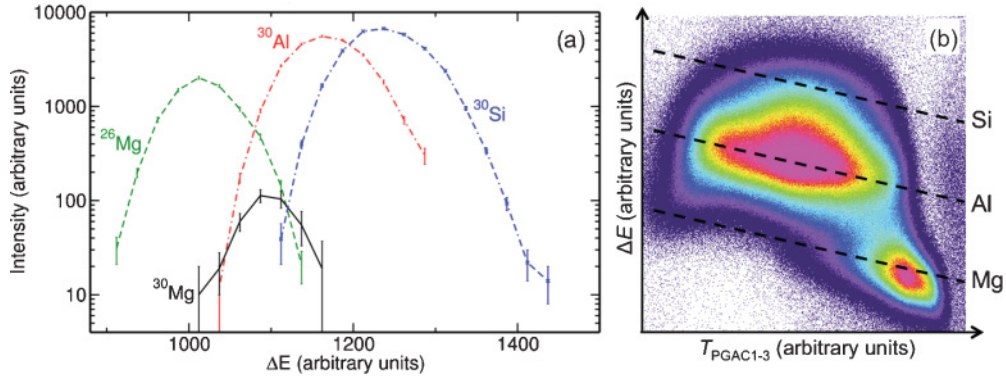

FIG. 1. (Color online) (a) Intensity of the transitions feeding directly the ground states of ^{26,30}Mg, ^{30}Al, and ^{30}Si, plotted as a function of the energy loss in the first ion chamber, ΔE. (b) Two-dimensional histogram of ΔE versus time of flight between the first and third PGACs, $T_{\mathrm{PGAC1–3}}$. The approximate locations of recoil groups of different Z are indicated by dashed lines.

technique. The population of ^{30}Mg through fusion-evaporation provides access to states of higher energy and spin than have been studied previously. Furthermore, the high degree of alignment inherent in this reaction mechanism, along with the high efficiency and resolution of the detectors used, allows spin assignments to be made. Results for ^{30}Al and ^{30}Si, obtained in the same experiment, are presented elsewhere [12].

II. EXPERIMENT

The Argonne Tandem Linear Accelerator System delivered ^{18}O projectiles, at an energy of 37 MeV, onto a ^{14}C target of 70 μg/cm^2 thickness. The target was isotopically enriched to around 90%, the main contaminant being ^{12}C. Prompt γ decays at the target position were detected by the Gammasphere array [13], containing 101 Compton-suppressed Ge detectors. Reaction products were dispersed by the Fragment Mass Analyzer (FMA) [14] according to their mass-to-charge ratio, A/q. Slits were introduced at the exit of the first electric dipole to reduce the transmission of scattered beam and other contaminant residues. Slits were also placed around the $A = 30$ recoil group at the focal plane; however, this also allowed transmission of some $A = 26$ residues, owing to a charge-state ambiguity (26/7). Behind the FMA was a combination of detectors, comprising three parallel-plate gridded avalanche counters (PGACs), interspersed by two transmission ion chambers (TICs), with a regular ion chamber at the back. Further details of this multidetector system are given in Ref. [15]. Gas pressures inside the three ion chambers were set such that ^{30}Mg recoils were brought to rest in the final chamber. The data-acquisition system was triggered by the detection of at least one γ ray in Gammasphere in coincidence with the arrival of an ion with $A/q = 30/8$ at the first PGAC. A total of 2.3×10^6 events were recorded over a period of around 130 h.

Energy-loss data from the three ion chambers were used to provide Z identification and to remove any remaining scattered beam. The intensities of the ground-state feeding transitions in ^{26,30}Mg, ^{30}Al, and ^{30}Si, are plotted as a function of the energy loss in the first TIC, ΔE, in Fig. 1(a). This figure shows that the strongest transition in ^{30}Mg is not only two orders of magnitude less intense than the corresponding γ rays in ^{30}Si and ^{30}Al, but that the overlap of the different Z groups is such that any gate in ΔE around the ^{30}Mg group brings in significant ^{30}Al and ^{26}Mg contamination. The ^{26}Mg and ^{30}Mg products do not have the same range of ΔE values owing to different reaction kinematics. Figure 1(b) provides a spectrum of ΔE against the time of flight between the first and third PGACs, $T_{\mathrm{PGAC1–3}}$. Recoils lie along downward sloping lines according to their Z value, while mass decreases with increasing $T_{\mathrm{PGAC1–3}}$ along these lines. Thus, the high-intensity recoil group in the lower right-hand corner is predominantly ^{26}Mg residues, whereas the ^{30}Mg group should be found toward the lower-middle of the plot, directly below the Al and Si groups.

It is possible to place different polygonal gates on this two-dimensional plot and produce coincident γ-ray spectra. Cross contamination between spectra can be minimized using a normalized subtraction procedure. An example is given in Fig. 2, where panel (a) contains a spectrum formed by gating on the expected location of ^{30}Mg recoils in Fig. 1(b). This spectrum is dominated by transitions in ^{30}Al. Figure 2(b) presents a subtraction of an ^{30}Al-gated spectrum from that in panel (a), after being normalized to attempt to remove the contaminant ^{30}Al lines. In this subtracted spectrum, there is still some contamination, mainly from transitions in ^{30}Si. However, the procedure removes sufficient levels of contamination from the more prolific exit channels of the reaction so that several new photopeaks can be identified as originating from ^{30}Mg, with energies 802, 985, 1060, 1481, 1816, 1898, and 1975 keV.

A recoil-gated $\gamma\gamma$ coincidence matrix enabled further investigation of the new transitions and the construction of a ^{30}Mg level scheme. Figure 3 provides examples of $\gamma\gamma$ spectra from this matrix; note that the addition of a γ-ray condition provides further selectivity, removing all Al and Si contamination.

The photopeak resolution in the ^{30}Mg γ-ray spectra was improved by the use of an event-by-event Doppler correction. Owing to the restrictive opening angle of the FMA (8 msr), recoils that are transmitted to the focal plane tend to fall into two groups: those given a momentum boost up, or down,

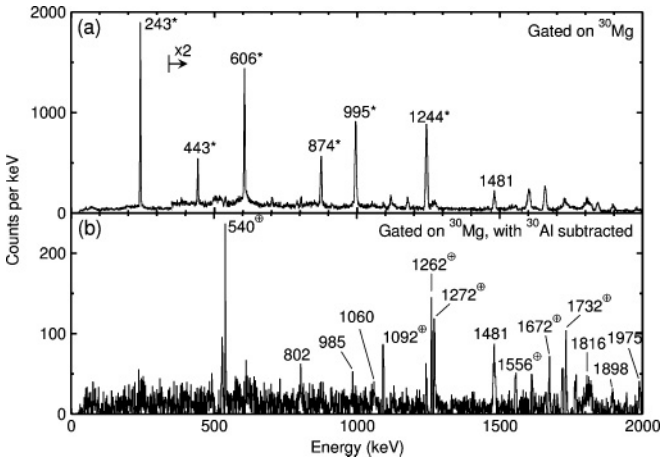

FIG. 2. γ-ray singles spectra formed by gating on different groups in the ΔE vs $T_{\mathrm{PGAC1-3}}$ plot. (a) The coincidence gate corresponds to the expected location of ^{30}Mg (note the change in intensity scale at 350 keV). (b) Normalized subtraction of ^{30}Al-gated spectrum from spectrum (a). Photopeaks are labeled by their energy in keV. Peaks labeled with an asterisk are known to originate from ^{30}Al, while those observed in ^{30}Si are marked with a ⊕. See text for further details.

the beam line by particle evaporation. Use of an average recoil velocity in the Doppler correction can, therefore, prove unsatisfactory. Here the recoil velocity was deduced on an event-by-event basis from the time of flight between the first and third PGACs, $T_{\mathrm{PGAC1-3}}$. Comparing the energies of ^{30}Mg photopeaks in uncorrected spectra, ring by ring, the value of the recoil velocity β was deduced. A fit to these data established the relationship between β and $T_{\mathrm{PGAC1-3}}$ for each of the recoil groups, and this function was subsequently used to correct γ-ray energies on an event-by-event basis. The resulting Doppler correction improved the resolution of the observed photopeaks in ^{30}Mg by around 10%, compared to that obtained using a single average recoil velocity.

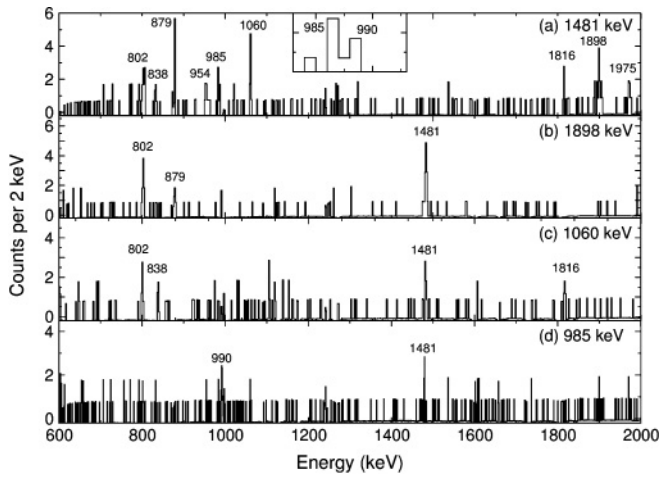

FIG. 3. Sample γ-ray coincidence spectra for ^{30}Mg events, formed from a gate in the plot of ΔE vs $T_{\mathrm{PGAC1-3}}$. The spectra are additionally gated on γ-ray energies of (a) 1481 keV, with the inset showing the region around the 895/990-keV doublet on a larger scale; (b) 1898 keV; (c) 1060 keV; and (d) 985 keV.

A level scheme for ^{30}Mg was constructed using coincidence relationships, energy, and intensity sums, and spins were assigned on the basis of an angular-distribution analysis. Efficiency-corrected γ-ray intensities were measured in nine spectra, corresponding to each of the different values of $\cos^2\theta$ in the Gammasphere array. These intensities were then fitted with the function

$$W(\theta) = A_0\,[1 + a_2 P_2(\cos\theta) + a_4 P_4(\cos\theta)]\,, \qquad (1)$$

where $P_L(\cos\theta)$ are Legendre polynomials. For some transitions, statistics proved insufficient for ring-by-ring angular distributions to be measured. In these cases, a two-point measurement was taken, by summing the spectra from detectors at angles 32°, 37°, 143°, 148°, and 162° and those at 79°, 81°, 90°, 99°, and 101°. A ratio R_{ang} of the intensity at these two sets of angles was then used as an indication of the possible multipolarity of transitions of interest. It is important to note that assigning spins to excited states on the basis of R_{ang} inevitably leads to a loss of sensitivity to the a_4 coefficient, as the procedure averages detector angles around either 0° and 180° or 90° and also does not allow clear distinction in the case of mixed transitions (discussed in more detail in what follows).

III. RESULTS

The level scheme for ^{30}Mg deduced from the current work is presented in Fig. 4. Properties of the excited states and transitions are given in Table I. Of the 11 transitions in Fig. 4, only 2 have been reported previously with the same

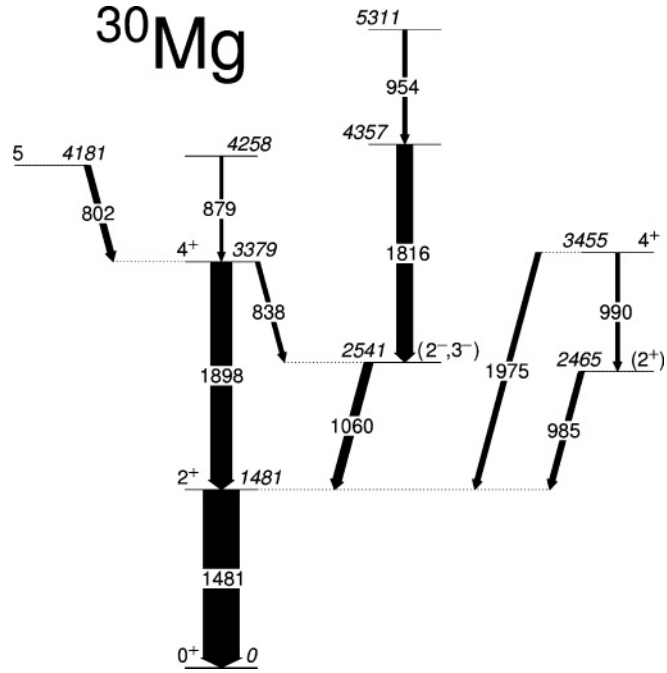

FIG. 4. Excited states and transitions in ^{30}Mg. Energies are given to the nearest keV. The thickness of the arrows is proportional to the intensity of the γ rays. Parentheses indicate tentative spin and parity assignments. The apparent intensity mismatch to and from the state at 2541 keV is not significant given the experimental error, as discussed in the text.

TABLE I. Excited states and transitions in ^{30}Mg, as deduced in the current work. Energies are in keV; intensities are normalized to 100. Angular distribution coefficients a_2 and a_4 are defined in Eq. (1); the angular ratio $R_{\rm ang}$ is defined in the text as well.

$E_{\rm level}$	J^π	E_γ	I_γ	a_2	a_4	$R_{\rm ang}$
1481	2^+	1480.6(5)	100(6)	+0.44(10)	−0.33(14)	0.55(7)
2465	(2^+)	984.8(17)	16(4)			2.4(19)
2541	$(2^-, 3^-)$	1059.8(9)	25(9)			0.34(24)
3379	4^+	838.4(3)	12(4)			
	4^+	1898.4(8)	59(5)	+0.68(23)	−0.37(29)	0.55(13)
3455	4^+	1974.8(19)	15(5)			0.61(26)
		990.0(5)	11(3)			
4181	5	802.3(6)	17(2)	−0.53(26)		1.86(61)
4258		879.0(9)	8(3)			
4357		1816.0(23)	44(26)			
5311		954.0(15)	12(2)			

placement as presented here. Following β decay [16,17] and β-delayed neutron emission [18], a 1481-keV transition has been observed feeding the ground state, and the 985-keV line was also placed in these studies. The latter study had argued a spin parity of 2^+ for the state at 1481 keV and tentatively for the state at 2465 keV.

Owing to low statistics and a high degree of contamination from transitions in ^{30}Al and ^{30}Si, full angular distributions, as described earlier, could only be measured for the 1481-, 1898-, and 802-keV γ rays. For the remaining lines, analysis of the angular ratio $R_{\rm ang}$ was performed. A ratio <1 suggests a stretched quadrupole character, whereas $R_{\rm ang} > 1$ signifies a stretched dipole nature. Consistent assignments were obtained for the three transitions where both angular distributions and ratio measurements were possible. The state at 3455 keV is given a 4^+ assignment, on the basis of the 1975-keV γ ray, for which $R_{\rm ang} = 0.61(26)$.

The 2465-keV state was given a tentative 2^+ assignment in a previous study [18], on the basis of the $B(E2)$ value, and systematics with the decay pattern of the 2_2^+ state in ^{28}Mg. The large uncertainty on $R_{\rm ang}$ for the 985-keV transition in the current work makes it difficult to make a robust assignment, so the previous tentative $J^\pi = 2^+$ assignment is adopted here. Feeding this state is a transition with an energy of 990 keV. The proximity of this line to the 985-keV transition, and a contaminant 995-keV γ ray in ^{30}Al, make it difficult to extract any angular information. However, it is placed here on the basis of the spectrum resulting from a gate at 985 keV [Fig. 3(d)] and the compliance of the energy sum with the parallel 1975-keV decay route, which lies within 1σ. The assignments of the states at 3455 and 2465 keV, discussed earlier, suggest an $E2$ character for the weak 990-keV transition. The difference in energy of the 990- and 1975-keV lines is then responsible for the relative branching ratio from the 3455-keV level.

The 1060-keV transition also has $R_{\rm ang} < 1$, indicating that a 4^+ assignment may also be appropriate for the 2541-keV level. However, such an assignment would make this level yrast by 0.8 MeV, which would be expected to attract significantly greater feeding than is evident from the observed γ-ray intensities. It seems likely, therefore, that this transition is of mixed character, with $\Delta J = 0$ or 1, and a large mixing ratio, giving a subsequent assignment of spin $2\hbar$ or $3\hbar$ to the 2541-keV state. No angular ratio could be obtained for the weaker 838-keV transition. It is interesting to note that there is no evidence for the population of the 2541-keV state in β decay from the 2^+ ground state of ^{30}Na, whereas there is strong β decay feeding to the proposed 2^+ states at 1481 and 2465 keV [17,18]. The absence of such feeding to the level at 2541 keV would be consistent with a tentative assignment of negative parity.

It should be noted that the intensity of the 1816-keV γ ray may appear too large in Fig. 4, resulting in a loss of intensity at the 2541-keV state. However, as shown in Table I, the error on this intensity is greater than 50%, owing to a multiplet of contaminating transitions at this energy in ^{30}Al and ^{30}Si. The intensity sum rules are in fact consistent within the measured uncertainties.

The state at 4181 keV is given a firm spin assignment of $5\hbar$ on the basis of the angular-distribution measurements given in Table I. The latter do not allow distinction between $E1$ and $M1$ transitions, however, and no parity assignment is made to this state.

IV. DISCUSSION

To assist in the interpretation of the levels observed in ^{30}Mg, a series of shell-model calculations were performed using the code of Ref. [19], and the Monte Carlo shell model (MCSM) method [20]. The experimental levels are compared to the results of the calculations in Fig. 5.

An initial calculation was carried out using the Universal *sd* (USD) effective interaction [22,23] within a full *sd* model space, where lower shells were considered to be closed. The calculated energy levels are summarized in the second column of Fig. 5. For the shell-model states predicted to lie below ∼4.5 MeV, each calculated level has a potential partner in the experimental spectrum; the calculated 2_1^+ level at 1670 keV corresponds to the observed 2_1^+ state at 1481 keV, the calculated 2_2^+ state at 3470 keV corresponds to the observed state at 2465 keV, and the calculated 4_1^+ level corresponds to one of the two 4^+ states at 3379 or 3455 keV. Irrespective

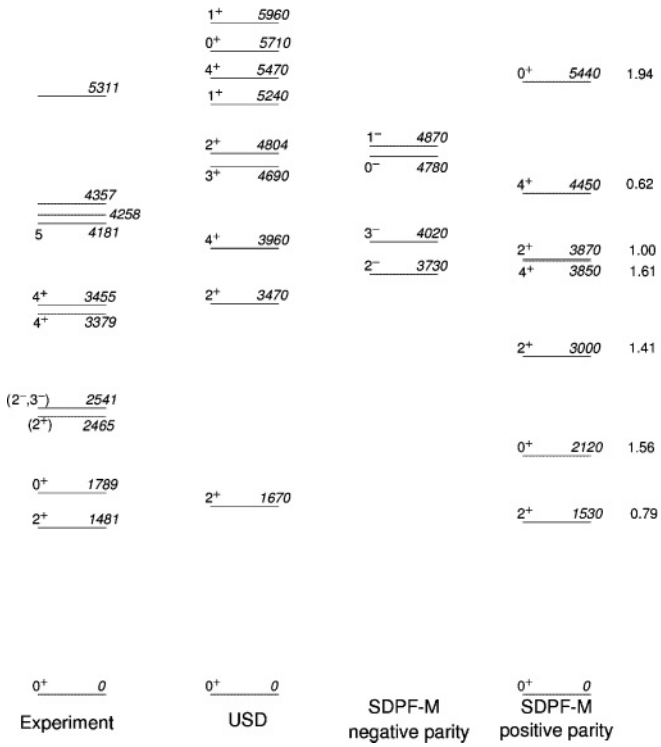

FIG. 5. Shell-model calculations for ^{30}Mg resulting from the USD and SDPF-M interactions, shown alongside the experimental levels deduced in this work, with the addition of an excited 0^+ state observed in Ref. [21]. Calculated energies are given to the nearest 10 keV. For the USD interaction and positive-parity SDPF-M calculations, the lowest two states of each spin are given. For the negative-parity levels, only the lowest of each spin up to 3^- have been calculated. The numbers on the right-hand side represent the average number of neutron excitations to the fp shell. See text for details.

of the detailed one-to-one comparison, the calculated states lie higher than those observed experimentally. There also appear to be additional observed states compared to the sd calculation. The experimentally observed 4^+ state at either 3379 or 3455 keV (depending on which one is the partner of the calculated 4^+_1 level) is unlikely to correspond to the calculated 4^+_2 level, which lies much higher in excitation at 5470 keV. The appearance of a likely negative-parity state at 2541 keV is clearly outside the USD calculations. A 0^+_2 state fed in β decay at 1789 keV [21], not observed in the current work, also does not have a reasonable USD counterpart. Both the overestimation of the excitation energy and the presence of additional low-lying experimental levels indicate that calculations within the sd model space are insufficient to account properly for excitations in ^{30}Mg, even at relatively low spin. Extensions to the model space are needed to generate more states, to produce counterparts for all experimental states, and increase the overall level of mixing, compressing the lowest-lying states in energy, to give a better match in energies.

Calculations beyond the sd model space were performed using the MCSM method [20], with the SDPF-M interaction, to judge the influence of excitations into the fp-shell orbitals. Within this $sd + f_{7/2} + p_{3/2}$ model space there are no further restrictions on the configurations considered. Further details can be found in Ref. [24]. This interaction has previously been used in calculations for a number of neighboring nuclei, including recent data on ^{31}Mg [25]. In this case, the interaction placed a $1/2^+$ state at 500 keV, which is taken as being analogous to the observed $1/2^+$ ground state. The interaction also successfully reproduces the measured g factor for ^{31}Mg, giving a result of -1.70, compared to the absolute experimental value of 1.7671(3).

The possibility of negative-parity assignments for the 2541-keV level, with tentative spin-parity of 2^- or 3^-, was considered by comparison with states calculated with an odd number of cross-shell excitations. The calculated negative-parity states lie above 3730 keV, as shown in the third column of Fig. 5. If indeed the arguments presented earlier for this tentative assignment are substantiated, it appears that the shell-model calculations overestimate the excitation energy of negative-parity excitations. Indeed, similar conclusions are also reached when considering the appearance of the non-USD states at low excitation energy, as discussed in what follows.

In a simple scenario, one of the observed 4^+ states at 3379 or 3455 keV is likely to arise from outside the sd space and is a candidate for the excitation of two particles into the fp shell. It is likely that the low-spin states at 2465 is of positive parity and is, therefore, also a candidate to involve similar excitations. More complex structures might arise if there is substantial mixing between 0p-0h and 2p-2h configurations. The presence of a γ-ray transition between the states at 3455 and 2465 keV may hint at a common structure for those levels, whereas the 2541-keV level is linked by transitions with the yrast sequence. To investigate these issues, the positive-parity states from the MCSM calculations are shown on the right-hand side of Fig. 5, where states are labeled by spin-parity, excitation energy, and N_{fp}, the average number of neutron excitations into the fp shell. A pure 0p-0h state would have $N_{fp} = 0$, whereas a pure 2p-2h state has $N_{fp} = 2$, if the contribution of 4p-4h are considered to be negligible.

The first excited state is calculated to lie just 49 keV above the observed level 2^+_1, a closer level of agreement than for the USD result. Its structure is predominantly 0p-0h with $N_{fp} = 0.79$, as might be expected. The presence of a strong transition to this level from the observed 4^+_1 state at 3379 keV suggests a similarity in structure. Therefore, the calculated 4^+ state at 4450 keV would appear to be the theoretical partner, even though the energy is overestimated (see comment in what follows). In a similar fashion, the calculated states at 3000 and 3850 keV, both with $N_{fp} \sim 1.5$, would appear to correspond to the observed 2^+_2 and 4^+_2 states at 2465 and 3455 keV, respectively. The calculated 0^+ level at 2120 keV may correspond to the 0^+_2 state reported by Schwerdtfeger *et al.* [21], observed via an $E0$ transition to the ground state, and with an excitation energy of 1789 keV. The calculations indicate a significant 2p-2h configuration for this state, consistent with the conclusions drawn in Ref. [21], where beyond-mean-field calculations indicate a large $f_{7/2}$ component for the 0^+_2 state.

The MCSM calculations appear to have several specific problems associated with the "intruder" excitations predicted at too high an excitation energy. This could be attributed

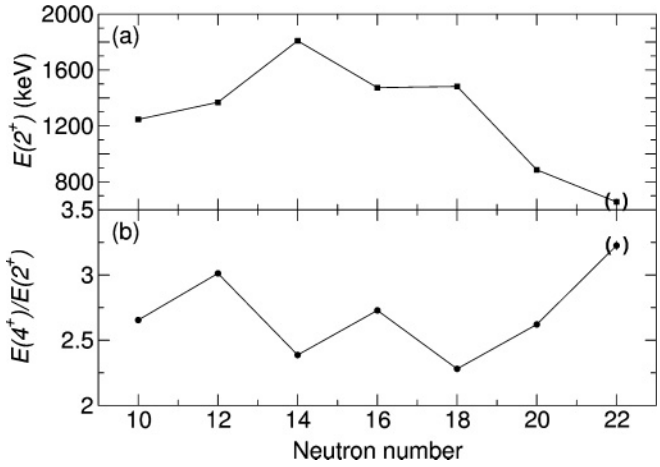

FIG. 6. $E(2_1^+)$ and $R(4_1^+/2_1^+)$ values as a function of neutron number for the even-even isotopes $^{22-34}$Mg. The $E(2_1^+)$ and $R(4_1^+/2_1^+)$ scales are offset by 2 and 600 keV, respectively. The brackets indicate tentative assignments; see text for comments on the sources of the data shown.

to overprediction of the excitation energy of the 2p-2h configurations and/or overestimation of the mixing between 0p-0h and 2p-2h excitations, pushing the predicted 2_2^+ and 4_2^+ excitation energies too high. The calculated 4_1^+ state also appears to have been pushed up by excessive mixing with the other 4^+ configuration. Indeed, the close proximity of the observed 4^+ states, which are less than 100 keV apart, seems to suggest that the mixing of these two states is minimal. Comparison of the tentative negative-parity state with the 1p-1h calculations may hint that the picture does need to include a reassessment of the energy of cross-shell configurations. There appears to be some potential to improve on the current shell-model calculations, in terms of both improving single-particle energies and interactions and extending the model space available to cross-shell configurations.

Given the firm assignment of $J^\pi = 4^+$ quantum numbers to the level at 3379 keV, a comparison can be drawn with the systematics of the low-lying states across the neutron-rich Mg isotopes. In particular, the energy of the first 2^+ state, $E(2_1^+)$, and its ratio with the 4_1^+ level energy, $R(4_1^+/2_1^+)$, are two quantities from which structural inferences are often gathered. These parameters are plotted in Fig. 6 for the even-even isotopes $^{22-34}$Mg. Some caution is needed in interpreting these data, as spin assignments in some of the heavier isotopes are tentative. In the case of ^{34}Mg, two strong γ-ray lines from two-step fragmentation studies have been tentatively associated with the decays of the 2_1^+ and 4_1^+ levels [26], with the latter assignment indicated by the authors as being less certain. For ^{32}Mg, recent (p, p') measurements to the 2321-keV state have angular distributions that are best reproduced with a $J^\pi = 4^+$ assignment [27]. Data for ^{30}Mg$_{18}$ are taken from the current work and, for the other isotopes, the low-lying states are well established (see, for example, Ref. [28]).

There is almost no change (<10 keV) in the $E(2_1^+)$ value between ^{28}Mg$_{16}$ and ^{30}Mg$_{18}$, in stark contrast with the sharp drop of around 600 keV when moving to ^{32}Mg$_{20}$. The values of $R(4_1^+/2_1^+)$, however, are 2.73 and 2.62 for ^{28}Mg and ^{32}Mg, respectively, but just 2.28 for ^{30}Mg. This value is the lowest of all the Mg isotopes in Fig. 6. While this is approaching the vibrational limit, it could also indicate the presence of a soft nuclear shape. Moving into the island of inversion, the ratio of energies appears to increase rapidly toward the rigid rotor limit at $A = 32$, consistent with the notion that the drop in energy of the fp orbitals does indeed increase collectivity, enabling a rotational-like sequence to appear. With the apparent softness of ^{30}Mg, it is perhaps not surprising that so many states appear at energies far lower than predicted by the shell-model calculations; it is clear that configurations involving the fp orbitals are involved at excitation energies as low as 2.5 MeV, indicating the level to which these intruder orbitals have fallen close to the sd shell at the periphery of the island of inversion.

V. CONCLUSIONS

The level scheme in Fig. 4 continues to illustrate the power of spectroscopy following $2p$ evaporation for the investigation of neutron-rich nuclei. In the current work spins are proposed on the basis of angular-distribution measurements. As a result, it has been possible to make the firm assignment of $J^\pi = 4^+$ to the state at 3379 keV, leading to a ratio $R(4_1^+/2_1^+)$ of 2.28. The failure of shell-model calculations, with the latest interactions for an extended sd-fp model space, to reproduce many of the experimental levels is an indication that 2p-2h cross-shell excitations play a role at relatively low excitation energies in this isotope. Therefore, the development of better interactions is paramount to increasing our understanding of nuclear structure in this region, as is the continued experimental exploration around the island of inversion.

ACKNOWLEDGMENTS

This work was supported by the US Department of Energy, Office of Nuclear Physics, under Contract No. DE-AC02-06CH11357, by the UK Science and Technology Facilities Council, by US National Science Foundation Grants No. PHY-01-01253, No. PHY-0456463, and No. PHY-07-56474, and by the Scottish Universities Physics Alliance. The authors are grateful to the group at Birmingham University for the loan of the ^{14}C target. DS acknowledges financial support from RIKEN.

[1] C. Thibault, R. Klapisch, C. Rigaud, A. M. Poskanzer, R. Prieels, L. Lessard, and W. Reisdorf, Phys. Rev. C **12**, 644 (1975).
[2] X. Campi, H. Flocard, A. K. Kerman, and S. Koonin, Nucl. Phys. A **251**, 193 (1975).
[3] G. Audi, A. H. Wapstra, and C. Thibault, Nucl. Phys. A **729**, 337 (2003).
[4] G. Huber *et al.*, Phys. Rev. C **18**, 2342 (1978).
[5] W. Geithner *et al.*, Phys. Rev. Lett. **101**, 252502 (2008).

[6] E. K. Warburton, J. A. Becker, and B. A. Brown, Phys. Rev. C **41**, 1147 (1990).
[7] T. Otsuka, R. Fujimoto, Y. Utsuno, B. A. Brown, M. Honma, and T. Mizusaki, Phys. Rev. Lett. **87**, 082502 (2001).
[8] T. Otsuka, T. Suzuki, M. Honma, Y. Utsuno, N. Tsunoda, K. Tsukiyama, and M. Hjorth-Jensen, Phys. Rev. Lett. **104**, 012501 (2010).
[9] J. R. Terry *et al.*, Phys. Rev. C **77**, 014316 (2008).
[10] S. J. Freeman *et al.*, Phys. Rev. C **69**, 064301 (2004).
[11] S. Zhu *et al.*, Phys. Rev. C **74**, 064315 (2006).
[12] D. Steppenbeck *et al.*, Nucl. Phys. A, doi:10.1016/j.nuclphysa.2010.07.010.
[13] I.-Y. Lee, Nucl. Phys. **520**, 641c (1990).
[14] C. N. Davids, B. B. Back, K. Bindra, D. J. Henderson, W. Kutschera, T. Lauritsen, Y. Nagame, P. Sugathan, A. V. Ramayya, and W. B. Walters, Nucl. Instrum. Methods B **70**, 358 (1992).
[15] C. L. Jiang *et al.*, Nucl. Instrum. Methods A **554**, 500 (2005).
[16] D. Guillemaud-Mueller, C. Detraz, M. Langevin, F. Naulin, M. de Saint-Simon, C. Thibault, F. Touchard, and M. Epherre, Nucl. Phys. A **426**, 37 (1984).
[17] P. Baumann *et al.*, Phys. Rev. C **39**, 626 (1989).
[18] H. Mach *et al.*, Eur. Phys. J. A **25**, s01 105 (2005).
[19] D. Morris and A. Volya, *Continuum Shell Model Calculations* (2010) [http://cosmo.volya.net].
[20] T. Otsuka, M. Honma, T. Mizusaki, N. Shimizu, and Y. Utsuno, Prog. Part. Nucl. Phys. **47**, 319 (2001).
[21] W. Schwerdtfeger *et al.*, Phys. Rev. Lett. **103**, 012501 (2009).
[22] B. H. Wildenthal, Prog. Part. Nucl. Phys. **11**, 5 (1984).
[23] B. H. Wildenthal, M. S. Curtin, and B. A. Brown, Phys. Rev. C **28**, 1343 (1983).
[24] Y. Utsuno, T. Otsuka, T. Mizusaki, and M. Honma, Phys. Rev. C **60**, 054315 (1999).
[25] M. Kowalska, D. T. Yordanov, K. Blaum, P. Himpe, P. Lievens, S. Mallion, R. Neugart, G. Neyens, and N. Vermeulen, Phys. Rev. C **77**, 034307 (2008).
[26] K. Yoneda *et al.*, Phys. Lett. B **499**, 233 (2001).
[27] S. Takeuchi *et al.*, Phys. Rev. C **79**, 054319 (2009).
[28] R. B. Firestone, *Table of Isotopes* (Wiley, New York, 1996), 8th ed.